NOVEL PHENOMENA IN TURBULENT ELLIPTIC WAKES

Masaru Kiya, Yukinobu Abe, Osamu Mochizuki and Hitoshi Ishikawa
Division of Mechanical Science, Hokkaido University
Sapporo 060-8628, Japan

ABSTRACT

Novel phenomena have been found in the wake of an elliptic disk set normal to the uniform approaching flow. There exist two periodic components of velocity fluctuations in the wake. One is centred around the minor plane, being due to alternate shedding of hairpin-like vortices. The other is centred around the major plane, being due to a meandering motion of the hairpin-like vortices. The axis switching, which is similar to that in ellitic jets (Ho & Gutmark 1987), occurrs at approximately 4 minor diameters downstream of the disk. Mechanism of the axis switching is completely different from that in the elliptic jets, being likely to be due to difference in growth rates of fundamental Fourier modes of global instability in the minor and major planes. Structure of the wake is studied by flow visualization, a direct numerical simulation, and a survey of the time-mean velocity and turbulence intensities.

INTRODUCTION

Wakes of three-dimensional bluff bodies have been studied mostly for axisymmetric ones such as spheres and circular disks. In the wakes of the axisymmetric bodies, there are three modes of instability (Berger et al. 1990). The first is the shear layer instability near the separation edge. The second is the pumping mode which is manifested as an axisymmetric oscillation of the recirculation zone behind the body. The third, which is the major mode of instability, is a helical mode, generating a helical vortex structure in the wake. Monkewitz (1988) argues that the frequency of periodic velocity fluctuations in the wake of a sphere is associated with the helical mode of instability in the axisymmetric steady near wake. The helical structures in the wake of a sphere are experimentally demonstrated by Taneda (1978), Berger et al. (1990) and Cannon et al. (1993). Hairpin-like vortices are also observed in the wake of a sphere (Achenbach 1974; Sakamoto & Haniu 1990; Shirayama 1992).

There are a number of asymmetric bodies in engineering applications. A typical example is the side-view mirrors of cars. However, the structure of turbulent wakes of asymmetric bodies is not clarified yet, at least to the same extent as that of the axisymmetric wakes.

The purpose of the present paper is to study the turbulent wake of an elliptic disk which is set normal to the approaching flow. The elliptic disk is chosen as a simple shape of asymmetric bluff bodies. This has two length scales and smooth variation of curvature along the edge. The latter is not the case for a rectangular plate, which is another simple shape of asymmetric bodies.

Apart from engineering applications, the turbulent wake of the elliptic disk deserves study in its own right. A few issues of interest are as follows. Is there any periodic vortex shedding form the disk? If any, what is the typical frequency or frequencies? What is the mechanism of the vortex shedding? Is there any axis switching in the wake as in an elliptic jet? If any, is the mechanism the same as that for the elliptic jet? These issues will be resolved in this paper. Moreover, the turbulence structure in the wake is presented by a survey of the time-mean velocities, turbulence intensities and Reynolds shear stresses.

EXPERIMENTAL APPARATUS AND METHODS

Flow configuration and definition of main symbols are shown in Figure 1. The x-axis is in the longitudinal direction, the y-axis along the major axis, and the z-axis along the minor axis; the origin is at the centre of the front face of the disk. The time-mean and fluctuating velocity components in the x direction are denoted by U and u. The r.m.s. value of u will be denoted by u'. The (x, y) plane will be referred to as the major

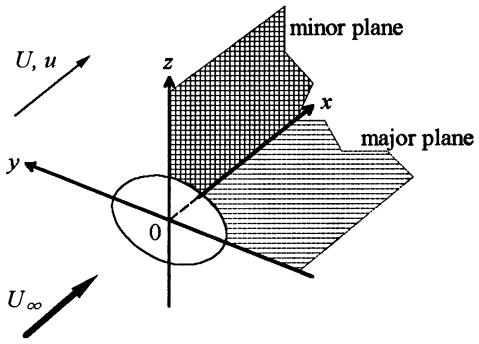

Figure 1. Elliptic disk, coordinate system , major and minor planes, and velocity components.

plane, while the (x, z) plane as the minor plane.

Experiments were performed in a through-flow wind tunnel with a 30.0 cm wide, 30.0 cm high and 100.0 cm long working section. The free-stream turbulence level is 0.5% at a main-flow velocity U_∞ of 15.0 m/s, which is employed in the present study.

Two elliptic disks of minor diameter D = 20.0 mm and major diameter L = 40.0 mm and 60.0 mm were manufactured from a brass plate of 3.0 mm in thickness, being bevelled by 45.0°. These disks will be referred to by the aspect ratio AR (= L/D), which is 2.0 and 3.0, respectively. The elliptic disk was fixed at 0.30 m downstream of the inlet in the middle of the working section by three steel wires of 0.2 mm diameter. The blockage ratio of the disks is 0.70-1.0%, so that their effects on the wake can also be neglected. No sensible oscillation of the disks was observed during the experiment at the main-flow velocity U_∞ = 15.0 m/s.

Measurements of the velocity components were made by constant-temperature hot-wire anemometers (KANOMAX Model 1010 and Model 1011) using I-wire probes and a split-film probe (TSI Model 1287) which can detect instantaneous flow reversal. The I-wire probes were employed only in regions of insignificant intermittent reverse flow. In the region of intermittent reverse flow, the velocity components U and u were detected by the split-film probe. Most of the velocity measurements were made in the major and minor planes.

No corrections were made for the effects of high turbulence intensities on the time-mean and fluctuating velocities, so that results within the band $0.3 < u'/U < 0.5$ should be taken with reserve (Chandrsuda & Bradshaw 1981). Measurements of U and u' in the major and minor planes at x/D = 2.0 and 8.0 by the I-wire probe and the split-film probe revealed that the mean deviation among measured values was within $\pm 0.05U_\infty$ and $\pm 0.02U_\infty$, respectively, in regions where the reverse-flow time fraction Ir was less than 0.2.

The wind-tunnel experiments were made at Reynolds number Re (= $U_\infty D/\nu$, ν: kinematic viscosity) of 20,000. Flow visualization by fluorescent dye was also made in a water channel at a lower Reynolds number Re = 200 to help the interpretation of results of the wind-tunnel experiments.

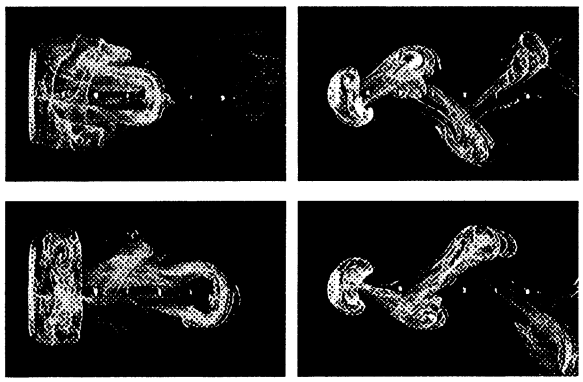

Figure 2. Flow visualization by fluorescent dye at Re = 200 in (a) major plane and (b) minor plane for AR = 3.0. Flow from left to right. Time advances from top to bottom with interval of $3.0D/U_\infty$, which is approximately one-third of vortex-shedding period. Flow patterns in (a) and (b) are not simultaneous.

RESULTS

Flow Visualization

The flow visualization for AR = 3.0 shows alternate shedding of large-scale vortices, which are the hairpin-like vortices in the major plane (Figure 2). The hairpin-like vortices are likely to experience a meandering motion in the major plane, as will be discussed later. The flow pattern were basically the same for AR = 2.0.

One might expect that an elliptic vortex ring is shed from the edge, generating the hairpin-like vortices by the self-induced deformation and interaction between neighboring vortex rings as in the case of the elliptic jets (Ho & Gutmark 1987; Hussain & Husain 1989). If this interpretation were correct, the deformed vortex ring should have two planes of symmetry, as shown in Figure 26 in Hussain & Husain (1989). The hairpin-like vortices in the wake have no such symmetry. This strongly suggests that the formation of the hairpin-like vortices and their alternate shedding have nothing to do with the self-induced deformation of the elliptic vortex rings but are associated with instability of flow in the near wake.

Vortex Shedding Frequencies

The shedding of the hairpin-like vortices in Figure 2 is periodic. This is demonstrated by the power spectra of longitudinal velocity fluctuations in the outer part of the wake for the disk of AR = 3.0 (Figure 3). The spectrum in the minor plane has a sharp peak at a frequency of 80 Hz; this frequency will be denoted by F_m. It is surprising that the spectrum in the major plane also has a definite peak at a lower frequency of 45 Hz; this frequency will be denoted by F_M. In the middle of the major and minor planes, the spectrum has two peaks at the frequencies F_m and F_M. These spectrum peaks were detected as far as x/D = 20. The spectrum peaks are also found for AR = 2.0, the peak frequencies being F_m = 90 Hz and F_M = 60 Hz.

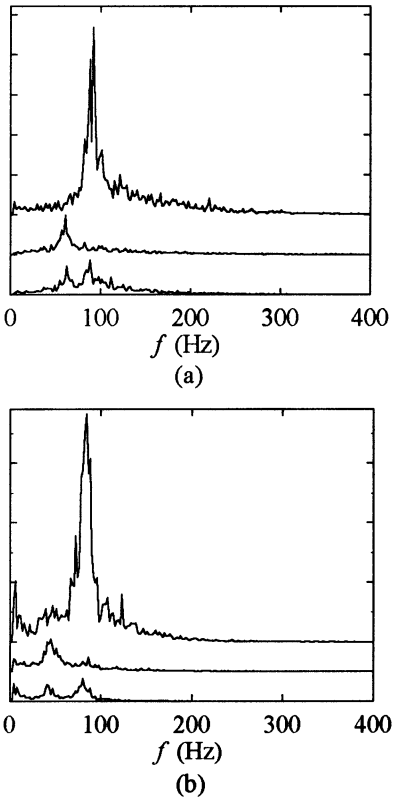

Figure 3. Power spectrum of longitudinal velocity fluctuation at x/D = 4.0 for (a) AR = 2.0: top curve at (y/D, z/D) = (0.0, 2.0) in minor plane; middle curve at (y/D, z/D) = (2.0, 0.0) in major plane; bottom curve at (y/D, z/D) = (1.5, 1.5), and (b) AR = 3.0: top curve at (y/D, z/D) = (0.0, 2.5) in minor plane; middle curve at (y/D, z/D) = (2.5, 0.0) in major plane; bottom curve at (y/D, z/D) = (2.0, 2.0). Vertical scale is arbitrary linear.

Structure responsible for the frequency F_M is not obvious in the flow visualization (Figure 2). This might be due to the difference in Reynolds numbers in the flow visualization (Re = 200) and the wind-tunnel experiment (Re = 20,000); that is, this structure might become evident at sufficiently high Reynolds numbers. It is also possible that the component F_M is due to a meandering motion of the wake in the major plane. This structure will be discussed later.

The frequencies F_m and F_M are plotted against AR in Figure 4 in the form of Strouhal number $St_i = F_iD/U_\infty$, where the suffix i implies M or m; the solid lines are drawn taking into account the branch of Sti extended to AR < 1. The data in Figure 4 show that no universal Strouhal number is likely to be constructed by merely adjusting the geometrical length scales D and L.

For the purpose of reference, the power spectrum was measured for thin rectangular plates normal to the main flow in the same wind tunnel. The spectra in minor and major planes were found to have a sharp peak at different

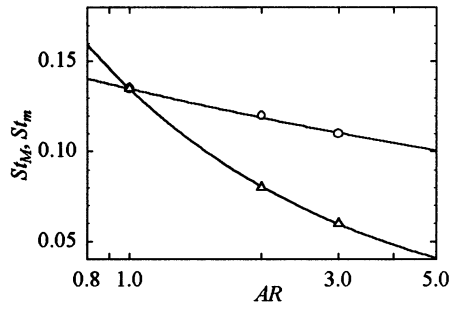

Figure 4. Strouhal numbers of elliptic disks as function of aspect ratio AR. ○, St_m; △, St_M. Solid lines are drawn taking into account the extended branch in AR < 1.

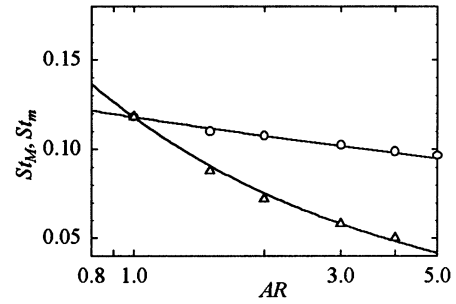

Figure 5. Strouhal numbers of rectangular plates as function of aspect ratio AR. ○, St_m; △, St_M. For meaning of solid lines, see caption of Figure 4.

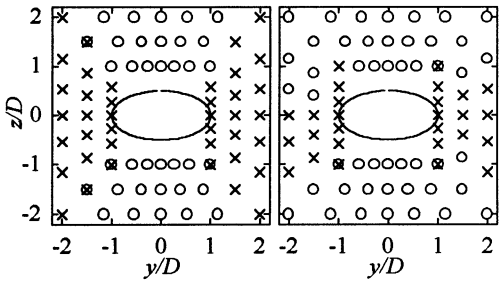

Figure 6. Distribution of St_M and St_m in cross-sections normal to main-flow direction for elliptic disk of AR = 2.0. ×, St_M; ○, St_m. Left, x/D = 2.0; right, x/D = 6.0.

frequencies. These frequencies in the form of St_m and St_M are shown in Figure 5 as a function of AR, in which D and L are the length of the shorter and longer sides, respectively. The Strouhal numbers have the same trend of change and approximately the same value as those for the elliptic disks. This suggests that the mechanism of generation of the periodic components is the same for both the elliptic disk and rectangular plate. Strouhal numbers St_M and St_m have distribu-tions in (y, z) cross sections such as shown in Figure 6. In the vicinity of

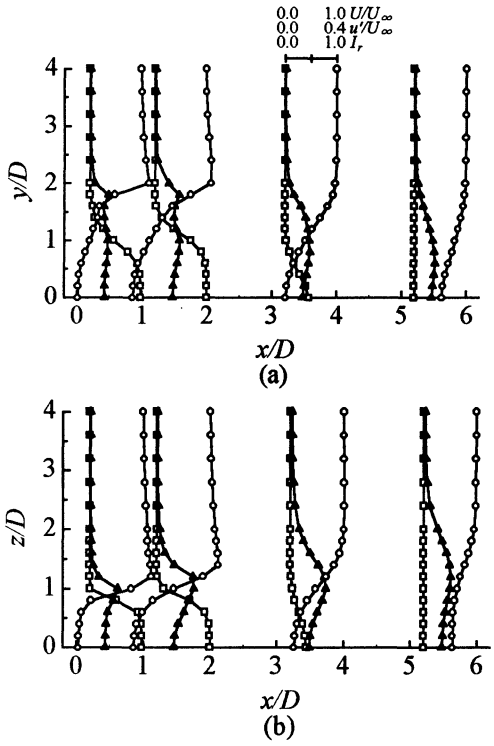

Figure 7. Distributions of U, u' and I_r measured by split-film probe in (a) major plane and (b) minor plane for AR = 3.0. ○, U; △, u'; □, I_r.

the disk x/D = 2.0, St_m is observed in a region centered around the minor plane while St_M appears in a region centered around the major plane. Farther downstream, the region of St_M shrinks while the region of St_m enlarges. Thus the hairpin-like vortices in the minor plane are likely to be the dominant structure in the near wake. The same features were also observed in the wake of the rectangular plates (not shown).

Flow Fields

Distributions of the time-mean velocity U, turbulence intensity u' and reverse-flow time fraction I_r in the major and minor planes are shown in Figure 7 for AR = 3.0. These were measured by the split-film probe. A plot of U on the wake axis against x (not shown) indicated that the end of the recirculating region is approximately at x/D ≈ 4.0. This was the same for AR = 2.0.

The level of u' is much higher in the minor plane than in the major plane in the region x/D < 5.0. This is due to the shedding of the hairpin-like vortices. The double peak of u' in the major plane at x/D = 1.0 and 2.0 is associated with two inflection points in the distributions of U.

The edge of the wake in the major plane remains approximately at the same position of y/D = 2.0, while that in the minor plane moves quickly outwards. This feature is

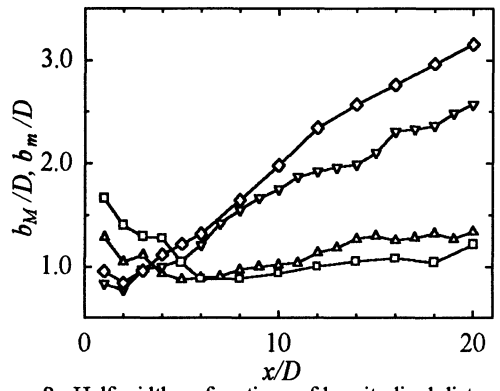

Figure 8. Half width as functions of longitudinal distance. △, b_M (AR = 2.0); ▽, b_m (AR = 2.0); □, b_M (AR = 3.0); ◇, b_m (AR = 3.0). Solid lines for visual aid only.

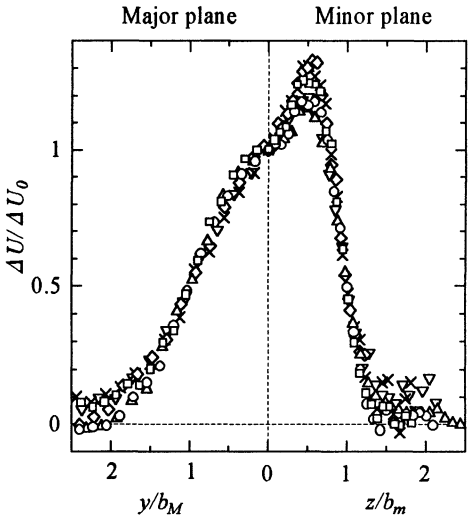

Figure 9. Distribution of velocity defect ΔU in major plane (on left) and in minor plane (on right). ▽, (x/D = 12.0, AR = 2.0); △, (12.0, 3.0); ×, (16.0, 2.0); ○, (16.0, 3.0); ◇, (20.0, 2.0); □, (20.0, 3.0). ΔU_0 is value of ΔU on the x-axis.

clarified in terms of half widths of the wake b_M and b_m in the major and minor planes, respectively, plotted against x in Figure 8. The cross-over of b_M and b_m occurs approximately at x/D = 3.8 for AR = 2.0 and x/D = 4.2 for AR = 3.0. This feature will be referred to as the axis switching. The axis switching is visualized as the rapid outward motion of the hairpin-like vortices in the z direction and at the same time as the shrinkage of these vortices in the y direction (Figure 2).

Similar axis switching has been observed in elliptic jets (Ho & Gutmark 1987; Hussain & Husain 1989). This is interpreted by the self-induced deformation of single elliptic vortex rings of the same aspect ratio. However, this mechanism

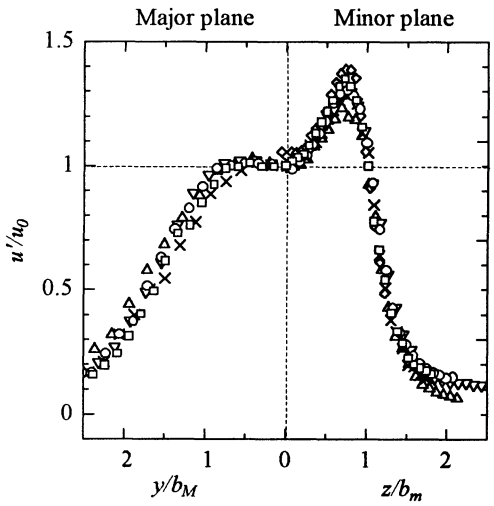

Figure 10. Distribution of terbulence intensity u' in major plane (on left) and in minor plane (on right). ▽, (x/D = 12.0, AR = 2.0); △, (12.0, 3.0); ×, (16.0, 2.0); ○, (16.0, 3.0); ◇, (20.0, 2.0); □, (20.0, 3.0). u'_0 is value of u' on the x-axis.

is not the case in the elliptic wakes. This is because the axis switching in elliptic jets has two planes of symmetry (Figure 26 of Hussain & Husain 1989) while the vortices in the minor plane of the elliptic wakes have no such symmetry. A possible mechanism of the axis switching in the elliptic wake will be discussed later.

The velocity defect ΔU in the wake is plotted in Figure 9 against the transverse coordinates normalized in the form y/b_M and z/b_m; the velocity defect is normalized by the velocity defect on the x axis ΔU_0. The velocity defect has approximately similar distributions in the region x/D = 12-20. The maximum velocity defect appears in the minor plane. Similar similarity was also found for the maximum u' (Figure 10).

Decay of Velocity Defect and Turbulence Intensity

Decay of the maximum velocity defect ΔU_{max} and the maximum turbulence intensity u'_{max} was not inconsistent with the decay law of the axisymmetric far wake $x^{-2/3}$ in the region x/D > 14 (not shown). This was also true for the equivalent half width be = $(b_M b_m)^{1/2}$, which obeys the law $x^{1/3}$ in the same region (not shown). This is reasonable because the statistical properties in the far wake has been assumed to depend only on the integral properties of the body such as the drag and lift. However, a large distance x appears to be needed in view of the significant difference in the profiles of ΔU in the major and minor planes (Figures 9).

DISCUSSION AND CONCLUSION

We conjecture that the mechanism responsible for the two periodic components is the global instability in the steady, recirculating near wake as in the case of the periodic vortex shedding in the near wake of two-dimensional bluff bodies

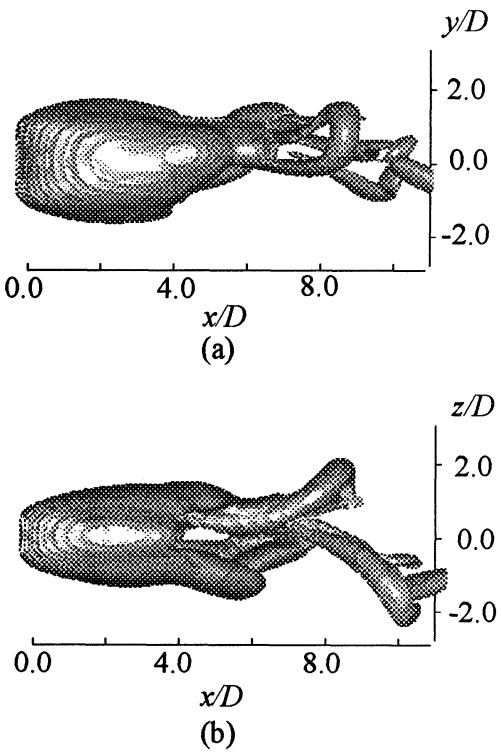

Figure 11. Vorticity contours in simulated wake of rectangular plate of thickness D/3 and aspect ratio AR= 2.0 at Re = 200 in (a) major plane and (b) minor plane.

(Huerre & Monkewitz 1990; Asai et al. 1996). If the Reynolds number is sufficiently low, a steady recirculating region is realized in the near wake of the disk. The velocity profile in the recirculating region has two representative length scales; one is the width of the wake in the minor plane, and the other is that in the major plane. The velocity profile in the minor plane is expected to have the fundamental mode of maximum growth rate at a critical Reynolds number. This eventually evolves into the alternate shedding of the hair-pin vortices (Figure 2). The same should also be the case in the major plane although the flow visualization has not demonstrated vortical structures associated with this mode.

The point is that the fundamental modes in the minor and major planes have different frequencies and growth rates. This is the reason why two periodic velocity components appear in the elliptic wake. The growth rate is greater in the minor plane than in the major plane. This is because the level of the velocity fluctuation u' in the region x/D < 6 is higher in the minor plane than in the major plane (Figure 7) and also because the region of the component F_M is eroded by that of the component F_m with increasing longitudinal distance in the same region (Figure 6).

If the above interpretation is correct, two periodic components are expected to appear also in the wake of a rectangular plate. This is the case as shown in Figure 5.

Moreover the Strouhal numbers for the elliptic disks are only slightly different from those for the rectangular plates at the same value of AR. This suggests that the velocity distribution in the steady recirculating region and thus the vortical structure caused by the instability are similar in the two wakes.

To examine the above conjecture on the instability, a direct numerical simulation of the wake of a rectangular plate was made by NAGARE3D.DH software produced by the Institute of Computational Fluid Dynamics Co. Ltd, Tokyo. This software employs a third-order upwind-difference scheme for the inertial terms. The rectangular plate has the thickness of D/3, D being the length of the shorter side, and the aspect ratio AR = 2.0. Reynolds number based on D is 200. The flow was impulsively started from rest with the velocity U_∞.

Figure 11 shows isosurfaces of magnitude of vorticity vector in the wake at the time $U_\infty t/D$ = 180.0. Hairpin-like vortices are alternately shed on both sides of the wake in the minor plane, while in the major plane these hairpin-like vortices appear to experience a meandering motion. Thus the structure responsible for the component F_M is this meandering motion. The meandering motion might be associated with large-scale vortices in the major plane although they are not clear in the simulation; these vortices might become clearer at higher Reynolds-numbers. The hairpin-like vortices emerge from the end of the recirculating region, not being a result of deformation of rectangular vortex rings which one might imagine are shed from the edge of the plate. Moreover, the power spectrum of velocity fluctuation u in the wake, which was obtained in terms of u during the time interval 167.0-203.8, was found to have a peak at the frequency close to F_M and F_m in the major and minor planes (not shown). These facts strongly suggest that the frequencies F_M and F_m are associated with the fundamental frequency of global instability in the near wake.

A comparison between Figures 2 and 11 reveals that the hairpin-like vortices emerge more downstream in the simulation than in the flow visualization. This is probably because the grid size for the simulation was not fine enough to capture details of the separated shear layer near the plate. Essential physics of the global instability in the recirculatin region, however, is likely to be captured by this simulation.

Figure 11 suggests that the axis switching is due to different growth rates of the fundamental mode of the global instability in the major and minor planes. The fundamental mode in the minor plane, which generates the hairpin-like vortices, has a greater growth rate than that in the major plane, thus quickly increasing the width of the near wake in the minor plane. This is likely to be supported by the fact that the heads of the hairpin-like vortices travel up to z/D = -2.4 or 2.2 in the region x/D = 8-10, while the meandering motion in the major plane moves the hairpin-like vortices towards the y-direction only to z/D = -1.1 or 1.5 in the same region. This causes the axis switching.

REFERENCES

Achenbach, E., 1974, "Vortex Shedding from Spheres," Journal of Fluid Mechanics, Vol. 62, pp. 209-221.

Asai, M., Nakagawa, H. and Nishioka, M., 1996, "Wake Instability and Frequency Selection of the von Karman Vortex Shedding," Journal of Japan Society for Aeronautical and Space Science, Vol. 44, pp. 251-256 (in Japanese).

Berger, E., Scholz, D. and Schumm, M., 1990, "Coherent Vortex Structures in the Wake of a Sphere and a Circular Disk at Rest and under Forced Vibrations," Journal of Fluids and Structures, Vol. 4, pp. 231-257.

Chandrsuda, C. and Bradshaw, P., 1981, "Turbulence Structure of a Reattaching Mixing Layer," Journal of Fluid Mechanics, Vol. 110, pp. 171-194.

Cannon, S., Champagne, F. and Glezer, A., 1993, " Observations of Large-cale Structures in Wakes behind Axisymmetric Bodies," Experiments in Fluids, Vol. 14, pp. 447- 450.

Ho, C.M. and Gutmark, E., 1987, "Vortex Induction and Mass Entrainment in a Small-aspect-ratio Elliptic Jet," Journal of Fluid Mechanics, Vol. 179, pp. 383-405.

Huerre, P. & Monkewitz, P.A., 1990, "Local and global instabilities in spatially developing flow," Annual Review of Fluid Mechanics 22, 473-537.

Hussain, F. and Husain, H.S., 1989, "Elliptic Jets. Part 1. Characteristics of Unexcited and Excited Jets," Journal of Fluid Mechanics, Vol. 208, pp. 257-320.

Monkewitz, P.A., 1988, "A Note on Vortex Shedding from Axisymmetric Bluff Bodies," Journal of Fluid Mechanics, Vol. 192, pp. 561-575.

Sakamoto, H. & Haniu, H., 1990, "A Study of Vortex Shedding from Spheres in a Uniform Flow," ASME Journal of Fluids Engineering, Vol. 112, pp. 386-392.

Shirayama, S., 1992, "Flow past a Sphere: Topological Transitions of the Vorticity Field," AIAA Journal, Vol. 30, pp. 349-358.

Taneda, S., 1978, "Visual Observation of the Flow past a Sphere at Reynolds Numbers between 104 and 106," Journal of Fluid Mechanics, Vol. 85, pp. 187-192.